Relation between composition and vacant oxygen sites in the mixed ionic-electronic conductors $La_{5.4}W_{1-y}M_yO_{12-\delta}$ (M = Mo, Re; $0 \leq y \leq 0.2$) and their mother compound $La_{6-x}WO_{12-\delta}$ ($0.4 \leq x \leq 0.8$)

Andrea Fantin[a], Tobias Scherb[a*], Janka Seeger[b], Gerhard Schumacher[a], Uta Gerhards[c], Mariya E. Ivanova[b], Wilhelm A. Meulenberg[b], Roland Dittmeyer[c] and John Banhart[d]

A detailed analysis of specimen composition, water uptake and their interrelationship in the systems $La_{6-x}WO_{12-\delta}$ ($0.4 \leq x \leq 0.8$) and $La_{6-x}W_{1-y}M_yO_{12-\delta}$ ($0 \leq y \leq 0.2$; M = Mo, Re) is presented. The three specimen series were investigated in dry and wet(D_2O) conditions. A systematic trend in mass loss and onset temperature variation was observed in $La_{6-x}WO_{12-\delta}$ ($0.4 \leq x \leq 0.8$). Even very small amounts (< 1 wt. %) of secondary phases were found to notably modify the specimen's water uptake and onset temperature of mass loss. The theoretical model for vacancy concentration available was used to calculate the vacant oxygen sites starting from mass loss values determined by thermogravimetry. A discrepancy between the calculated and observed concentration of vacant oxygen sites is observed for all three systems. The effect of substitution of W by Re or Mo on the vacancy amount is explained taking into account diffraction measurements and information on the oxidation state of the substituting elements Mo and Re.

[a]Department of Microstructure and Residual Stress Analysis, Helmholtz-Zentrum-Berlin GmbH, Hahn-Meitner-Platz 1, Berlin, 14109, Germany

[b]Institute of Energy and Climate Research, Forschungszentrum Jülich GmbH, Jülich, 52425, Germany

[c]Institute for Micro Process Engineering, Karlsruhe Institute of Technology, Hermann-von-Helmholtz-Platz 1, Eggenstein-Leopoldshafen, 76344, Germany

[d]Department of Applied Materials, Helmholtz-Zentrum-Berlin GmbH, Hahn-Meitner-Platz 1, Berlin, 14109, Germany

*correspondence email: tobias.scherb@helmholtz-berlin.de

1. Introduction

Hydrogen-related technologies could replace existing power generators running on fossil fuels. Instead of CO_2, the sole emission products of H_2-based engines would be water and heat, thus zero-emissions. The integrated gasification combine cycle in pre-combustion capture is just an example of how strongly related carbon capture and storage and H_2 production are in the context of restricted global pollution. In addition to the fact that H_2 is a zero-emission fuel, it has the highest energy density per unit mass amongst all fuels and is, therefore, suggested to be used as primary energy carrier for numerous applications [1-6]. A further advantage is that hydrogen gas can be produced from clean and renewable energy sources such as solar, wind and hydroelectric power through water electrolysis. Despite the fact that water electrolysis is the cleanest source for hydrogen production, natural gas reforming and coal gasification still are economically more favourable. However, hydrogen production from fossil fuels leads to various gas impurities such as CO_x, SO_x, NO_x and H_2O vapour, which restrict its use as a fuel of high purity. Therefore, highly efficient technologies in extracting highly pure H_2 out of a mixture of different gases need to be developed. At the same time, such technologies could also facilitate the capture and utilization of the other gas components such as CO_2 if they were to be separated concurrently with H_2-production (Carbon Capture and Utilization) for development of "green chemistry" [7, 8]. In this context, ceramic membranes for H_2/CO_2 separation drew much attention in the recent years, particularly in the development of stable materials with improved performance. Rare-earth tungstate-based materials are known to have high stability in acidic atmospheres [9-13]. In addition, with appropriate substitution for the W cations, the bulk H_2-permeation flow could substantially be increased [9, 10, 14, 15].

The aim of this work is to analyse in detail the water uptake of lanthanum tungstates (LWO), both non-substituted and substituted on W site by Mo and Re. Mo/Re atoms enhance the overall conductivity due to the increase of

electronic charge carriers, which make this compound more suitable for H_2-related technologies [9, 16, 17]. The determination of the structure details of lanthanum tungstates drew much attention in the recent years due to subtle distortions difficult to resolve univocally [18-25]. Finally, an agreement on the crystal structure has been recently reached [19, 20, 26, 27]. In 2016, the first publications on the detailed crystal structure of Mo/Re-LWO are appearing [19, 26, 27]. However, a systematic study on the water uptake and a comparison between theory and observation on LWO and Mo/Re-LWO systems is still missing. Only two different specimens belonging to the single-phase region of the non-substituted LWO system were investigated by Hancke, *et al.* [28]. They report that only one amongst the two compounds agrees with the most recent theoretical predictions. Water uptake properties of the Mo-LaWO system were presented by Amsif, *et al.* [29]. They showed, however, only two different Mo substitution levels (20 and 40 mol %) with cubic $Fm\bar{3}m$ structure. In this work, we present the results on a more relevant set of different specimens: seven LWO, $La_{6-x}WO_{12-\delta}$ ($0.4 \leq x \leq 0.8$), seven Mo-LWO and nine Re-LWO specimens $La_{5.4}W_{1-y}M_yO_{12-\delta}$ ($0 \leq y \leq 0.2$; M = Mo, Re), allowing for a deeper understanding of such systems. The structural model assumed for $La_{6-x}WO_{12-\delta}$ ($0.4 \leq x \leq 0.8$) and $La_{5.4}W_{1-y}M_yO_{12-\delta}$ ($0 \leq y \leq 0.2$; M = Mo, Re) was taken from recent literature, determined by different diffraction techniques [19, 26, 27].

2. Experimental

2.1. Samples

2.1.1. Synthesis

Powders of the sample series $La_{6-x}WO_{12-\delta}$ ($0.4 \leq x \leq 0.8$) were prepared by solid state reaction (SSR) while specimens of the sample series $La_{5.4}W_{1-y}M_yO_{12-\delta}$ ($0 \leq y \leq 0.2$; M = Mo, Re) were synthesized through the Pechini reaction [30]. Here, x and δ represent the deviations from the stoichiometry of the material family Ln_6WO_{12} (Ln = rare earth) reported in the 1960s and 1970s [31-33]. y represents the substitution on the W site by M = Mo, Re. The final sintering temperature for all prepared samples was 1500 °C for 12 h with heating and cooling rates of 2 K/min. Further details of the preparation of the two specimen series are given by Seeger, *et al.* [16].

2.1.2. Pre-treatment: dry(Ar) / wet-D_2O(Ar) specimens

The samples were pre-treated in a furnace under a continuous flow of either dried or humidified (D_2O) argon (Ar).The powder samples were placed in Al_2O_3 holders ($50 \times 20 \times 20$ mm^3). Drying was carried out at 900 °C for 4 h. Deuteration of 2.5 vol. % was achieved connecting two bubble bottles filled with D_2O to the argon pipe supplying the atmosphere to the furnace. The furnace was kept at 350 °C for 5 h.

2.2. Methods

2.2.1. Electron Probe Micro-Analysis

A JEOL JXA 8530F field emission microprobe was employed to measure the composition of the specimens. Epoxy-resin holders for samples and reference materials were used, whose surfaces were covered with carbon by evaporation

process. For each specimen 15 points were acquired, each one in different specimen regions and grains to improve the precision of the analysis. The following measurement specifications were used, voltage: 20 kV; electron current: 50 nA; beam diameter Ø: 2 μm or 500 nm (spot mode), depending on the grain size. Elemental maps were taken in a 45 x 45 μm^2 region at the same voltage. Images of the specimens were recorded in the back-scattered electron (BSE) mode prior to elemental maps acquisition.

2.2.2. Thermogravimetry

A Netzsch TG209F1 Iris micro-balance was used for thermogravimetric measurements to determine the water-uptake and loss of the specimens during heating. The mass-spectrometer QMS 403 Aëolos attached to the TG209F1 device allowed to measure ion currents. Between 150 mg and 300 mg of the sample material was loaded in Al_2O_3 crucibles. A heating ramp of 10 K/min from room temperature up to 1000 °C was employed. Prior to each measurement, the specimen chamber was evacuated twice and then purged with a stream of 50 ml/min argon gas for one hour. The measurements were performed under an Ar stream of 20 ml/min. The onset temperatures T_i were determined by linear interpolation and the mass loss was identified between the plateau at low and high temperatures. For further details see Fig. S3 in the Supporting Information.

2.2.3. X-ray diffraction.

X-ray diffraction (XRD) was performed in Bragg-Brentano geometry using a Bruker D8 Advance equipped with a LYNXEYE detector and a 0.5 μm thick nickel filter. Diffractograms were collected with the following specifications. Step: 0.01°; range: $10° \leq 2\Theta \leq 138°$; acquisition time: 4 s/step. The X-ray source was a copper tube, thus the characteristic radiation lines used were the Cu $K\alpha_1$ (1.5406 Å) and Cu $K\alpha_2$ (1.5444 Å). Phase identification was carried out with the ICDD PDF2 database in the EVA14 software. LeBail and Rietveld refinements were carried out using the software TOPAS [34] and GSAS with the EXPGUI graphical user interface [35].

3. Results and discussion

The XRD patterns of the LWO- and LW*M*O-dry(Ar) (*M* = Mo, Re) specimens are shown in the Supporting Information in Fig. S1 as a function of the scattering angle 2Θ ($10° \leq 2\Theta \leq 82°$), with peak indexing corresponding to a $Fm\bar{3}m$ space group (s.g.). From the peak indexing of Fig. S1 it can be recalled that

i. The lattice structure allow Miller indices *hkl* to become all odd or all even.

ii. The low-intensity reflections (e.g. for $2\Theta \leq 27°$, *hkl* = 111, 200, 220, 311) have been indexed according to the existence of a superstructure located at q = (½, ½, ½) of the reciprocal lattice vectors of the substructure. The substructure is a simple fluorite cell ($Fm\bar{3}m$ space group).

Point i justifies using the face-centred (*fcc*) unit cell due to the reflection conditions the *fcc* unit cell requires (*h*+*k*, *h*+*l*, *k*+*l* all even). Point ii justifies the doubled lattice parameters to account for the broken symmetry: the superstructure is commensurate as all the low-intensity reflections are located at simple fractions (half) of the

reciprocal lattice vectors of the substructure. Hence, the $Fm\bar{3}m$ space group with doubled lattice parameter as used for LWO in the literature is rationalized. For detailed structural studies on LWO, the reader is referred to [19, 26, 27] and to the Supporting Information, where the resulting crystal structure of $La_{5.6}WO_{12-\delta}$ is reported (see Fig. S2, *SI†*). Single-peak fitting and pattern simulations give an upper limit of 1 wt. % of $La_6W_2O_{15}$ for LWO52 and 1 wt. % of La_2O_3 for LWO56, respectively. Further details on the quantification of secondary phases in the LWO and LWReO systems investigated here are reported elsewhere [26]. The secondary phase peaks are shown with asterisks and sharps in Fig. S1 for La_2O_3 and $La_6W_2O_{15}$, respectively. In the LWMoO system less than 2 wt. % of La_2O_3 were estimated to be present in Mo10, Mo15 and Mo20(2) specimens (see Fig. S1c). In Table 1 an overview of all investigated samples is listed together with their label used in this work, the composition derived from EPMA, the refined lattice parameters for all dried and deuterated specimen and the amount and type of secondary phases.

Table 1. Nominal composition, sample labelling used throughout this work, composition from EPMA, lattice parameters of samples in the dry(Ar) and D2O(Ar) state and amount and type of secondary phases.

Nominal composition	Label	EPMA composition	a $_{dry}$ (Å)	a $_{D2O}$ (Å)	Secondary phases
$La_{5.4}WO_{12-\delta}$	LWO54P	$La_{5.56(3)}WO_{12-\delta}$	11.1733(1)	11.1825(1)	No
$La_{5.2}WO_{12-\delta}$ #	LWO52	$La_{5.36(4)}WO_{12-\delta}$ +	11.1687(1)	11.1736(1)	$La_6W_2O_{15}$ (< 1 wt. %)
$La_{5.3}WO_{12-\delta}$ #	LWO53	$La_{5.48(4)}WO_{12-\delta}$ +	11.1713(1)	11.1779(1)	No
$La_{5.4}WO_{12-\delta}$ #	LWO54	$La_{5.59(3)}WO_{12-\delta}$ +	11.1740(1)	11.1831(1)	No
$La_{5.45}WO_{12-\delta}$ #	LWO54.5	$La_{5.62(3)}WO_{12-\delta}$ +	11.1747(1)	11.1837(1)	No
$La_{5.5}WO_{12-\delta}$ #	LWO55	$La_{5.69(4)}WO_{12-\delta}$ +	11.1763(1)	11.1877(1)	No
$La_{5.6}WO_{12-\delta}$ #	LWO56	$La_{5.76(4)}WO_{12-\delta}$ +	11.1780(1)	11.1920(1)	La_2O_3 (< 1 wt. %)
$La_{5.4}W_{0.998}Re_{0.002}O_{12-\delta}$	Re02	$La_{5.67(3)}W_{0.997(1)}Re_{0.003(1)}O_{12-\delta}$	11.1751(1)	11.1864(1)	No
$La_{5.4}W_{0.995}Re_{0.005}O_{12-\delta}$	Re05	$La_{5.66(3)}W_{0.994(1)}Re_{0.006(1)}O_{12-\delta}$	11.1751(1)	11.1865(1)	No
$La_{5.4}W_{0.99}Re_{0.01}O_{12-\delta}$	Re1	$La_{5.61(3)}W_{0.990(2)}Re_{0.010(2)}O_{12-\delta}$	11.1746(1)	11.1845(1)	No
$La_{5.4}W_{0.95}Re_{0.05}O_{12-\delta}$	Re5	$La_{5.61(3)}W_{0.951(2)}Re_{0.049(2)}O_{12-\delta}$	11.1750(1)	11.1854(1)	No
$La_{5.4}W_{0.90}Re_{0.1}O_{12-\delta}$	Re10	$La_{5.65(6)}W_{0.899(5)}Re_{0.101(5)}O_{12-\delta}$	11.1787(1)	11.1911(1)	No
$La_{5.4}W_{0.85}Re_{0.15}O_{12-\delta}$	Re15	$La_{5.67(5)}W_{0.858(5)}Re_{0.142(5)}O_{12-\delta}$	11.1788(1)	11.1920(1)	No
$La_{5.4}W_{0.8}Re_{0.2}O_{12-\delta}$	Re20_IMP	$La_{5.66(7)}W_{0.845(7)}Re_{0.155(7)}O_{12-\delta}$	11.1778(1)	11.1881(1)	$La_6W_2O_{15}$ (< 3 wt. %), Re-rich phase
$La_{5.4}W_{0.8}Re_{0.2}O_{12-\delta}$	Re20	$La_{5.86(7)}W_{0.826(7)}Re_{0.174(7)}O_{12-\delta}$	11.1810(1)	11.1972(1)	No
$La_{5.4}W_{0.99}Mo_{0.01}O_{12-\delta}$	Mo1	$La_{5.62(3)}W_{0.992(1)}Mo_{0.008(1)}O_{12-\delta}$	11.1744(1)	11.1836(1)	No
$La_{5.4}W_{0.95}Mo_{0.05}O_{12-\delta}$	Mo5	$La_{5.64(3)}W_{0.953(2)}Mo_{0.047(2)}O_{12-\delta}$	11.1763(1)	11.1848(1)	No
$La_{5.4}W_{0.90}Mo_{0.1}O_{12-\delta}$	Mo10	$La_{5.8(5)}W_{0.89(2)}Mo_{0.11(2)}O_{12-\delta}$	11.1781(1)	11.1854(1)	$La_6W_2O_{15}$ (< 1 wt. %), La_2O_3 (< 2 wt. %)
$La_{5.4}W_{0.85}Mo_{0.15}O_{12-\delta}$	Mo15	$La_{5.8(2)}W_{0.85(1)}Mo_{0.15(1)}O_{12-\delta}$	11.1797(1)	11.1865(1)	$La_6W_2O_{15}$ (< 1 wt. %), La_2O_3 (< 1 wt. %)
$La_{5.4}W_{0.8}Mo_{0.2}O_{12-\delta}$	Mo20(1)	$La_{5.64(4)}W_{0.809(2)}Mo_{0.191(2)}O_{12-\delta}$	11.1791(1)	11.1838(1)	No
$La_{5.4}W_{0.8}Mo_{0.2}O_{12-\delta}$	Mo20(2)	$La_{5.64(7)}W_{0.803(7)}Mo_{0.197(7)}O_{12-\delta}$	11.1811(1)	11.1872(1)	$La_6W_2O_{15}$ (< 1 wt. %), La_2O_3 (< 1 wt. %)

solid state reaction; + composition scaled via Vegard`s law

Fig. 1 shows the La/(W+*M*) ratios of the investigated specimens as a function of *M*/(W+*M*) (*M* = Re, Fig. 1a; *M* = Mo, Fig. 1b). The compositions of the LW*M*O series measured with EPMA are indicated by filled green and blue squares for LWReO and LWMoO, respectively. The composition of the LWO series in Fig. 1a and Fig. 1b (open green squares) was determined through Vegard's law [36] and scaled to the composition of LWO54P measured with EPMA. An estimation of the single-phase region of LW*M*O is delimited by green dotted lines. On the right side of Fig. 1a, the single phase region boundaries ends at Re/(W+Re) ≈ 0.20. Above this value, a limit in the solubility of Re atoms in the LWO structure has been found [9, 16] (grey region in Fig. 1a). On the other hand, the LWMoO system presents a phase transition at Mo/(W+Mo) ≈ 0.40 from cubic ($Fm\bar{3}m$) to rhombohedral ($R\bar{3}$)[29]. Secondary phases were found in some samples (LWO52, LWO56, Re20_IMP, Mo10, Mo15, Mo20(2), see Fig. S1 and Table 1) by XRD and their main-phase compositions corrected accordingly (open red squares in Fig. 1). These phases were determined to be $La_6W_2O_{15}$ for data points below the single phase region and to La_2O_3 for data points above the single

phase region in Fig. 1, respectively. Due to the large uncertainties in La/(W+Mo) values in Mo10 and Mo15 specimens, the corrections on the main-phase composition values were neglected.

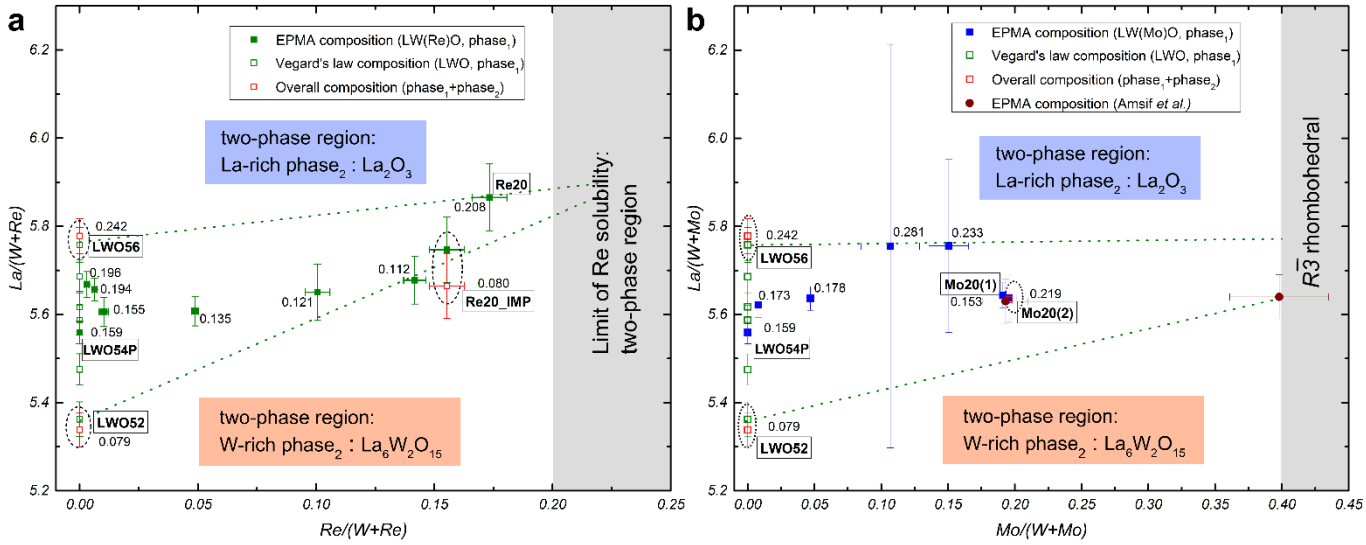

Fig. 1. La/(W+*M*) ratio as a function of substitution of W by *M* given as *M*/(W+*M*); *M* = Re, Mo. The region between the green dotted lines represents estimate for the presumed single-phase region of LW*M*O (*M* = Mo, Re) specimens. The mass loss (*Δm* in wt. %, reported next to the squares) has been measured by TG on humidified (D2O(Ar)) samples with an error of about 0.005 wt. % (95 % confidence level). The sample LWO54P is labelled in the figures, as well as LWO52, LWO56. Additionally, Re20_IMP and Re20, as well as Mo20(1) and Mo20(2) are labelled. In a) the grey region represents the limit of Re solubility in LWO reported in the literature [9, 16], while in b) the grey region represents where the LWMoO system undergoes a phase transition from cubic ($Fm\bar{3}m$) to rhombohedral ($R\bar{3}$) [29]. The filled brown circles are data points taken from Amsif, *et al.* [29], reported to be single phase.

In Fig. 2, the total mass (in wt. %) of LWO- and LW*M*O-D_2O(Ar) (*M* = Mo, Re) specimens as a function of temperature is depicted. In Fig. 2a, two related features are visible:

1. The increase of total mass loss Δm with increasing La/W ratio, and
2. The decrease of the onset temperature T_i with increasing La/W ratio.

Point 1 reflects the increasing concentration of oxygen vacancies in the crystal structure with increasing La/W ratio. These vacancies had been filled with O atoms / OD groups during the humidification pre-treatment. As the onset temperature T_i represents the thermal energy required for the first oxygen atoms and/or OD groups to leave the crystal structure, point 2 is related to the minimum energy required to create a vacancy. LWO52 shows the largest T_i (T_i^{LWO52} = 353(3) °C) value, which decreases slightly with increasing La/W ratio, where for instance T_i^{LWO53} = 345(3) °C and T_i^{LWO55} = 345(3) °C (see Fig. 2a and Fig. 3). Due to the presence of the secondary phase La_2O_3 in LWO56, its onset temperature (T_i^{LWO56} = 314(3) °C) and its Δm (Δm^{LWO56}) value are not representative. As T_i decreases with increasing La/W ratio, T_i decreases with increasing mass loss and thus with increasing vacancy concentration. Hence, a higher vacancy concentration in the specimen is related to a reduced stability of the crystal structure. It should be mentioned that the T_i values are determined during heating under dry conditions for heating ramps of 10 K/min and that they shift considerably to lower values with smaller heating rates.

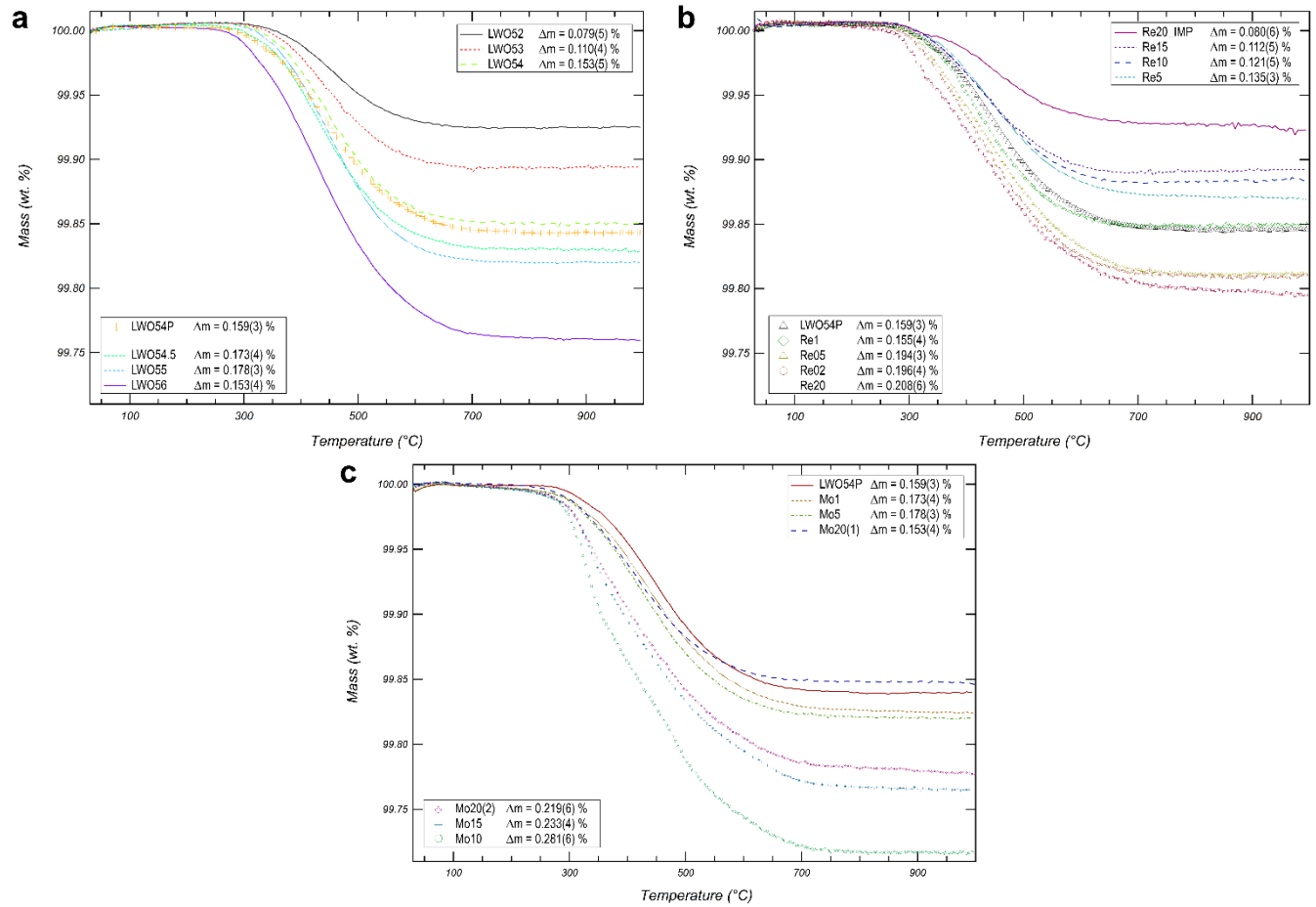

Fig. 2. Thermogravimetric curves of LWO- (a) and LW*M*O-D_2O(Ar) (*M* = Re (b), Mo (c)) specimens measured under dry(Ar) gas, where the mass (wt. %) is shown in dependence of the temperature. The colours used correspond to the colours used in Fig. S1. *Δm* values with a 95 % confidence level are summarised in the legends.

In Fig. 2b and Fig. 2c, the values of *Δm* as well as the onset temperatures T_i for LW*M*O are largely independent of the type and amount of substitution. According to Fig. 1, the La/(W+*M*) ratios need to be taken into account in order to understand *Δm* and T_i of LW*M*O. A detailed explanation in terms of vacancy concentration will be reported in the final part of this work along with the comparison between the three systems investigated. In Fig. 2b, the curve at the top (Re20_IMP, line) and the curve at the bottom (Re20, squares) deserve special attention. These TG curves follow a multiple-stage decay as manifested by various kinks and shoulders. The same reasoning applies for Mo10, Mo15 and Mo20(2) in Fig. 2c. This behaviour is rationalized by the presence of secondary phases, $La_6W_2O_{15}$ in Re20_IMP, and La_2O_3 in Re20, Mo10, Mo15 and Mo20(2). In Re20 and Mo20(2), originally single-phase, segregation of La_2O_3 occurred during repetitive annealing under reducing conditions at high temperatures (see Fig. S5, *SI†)*. Higher mass loss is revealed for La_2O_3-containing specimens compared to the phase-pure or $La_6W_2O_{15}$-containing specimens. The influence of the $La_6W_2O_{15}$ phase on the total *Δm* is negligible due to the similar mass loss of $La_6W_2O_{15}$ compared to the main LWO phase. However, the onset temperature of $La_6W_2O_{15}$ ($T_i^{La_6W_2O_{15}}$ = 252(3) °C) is much lower compared to the T_i of the main LWO/LW*M*O phase (see Table 2 and Fig. S4, *SI†*). This difference allows for assigning the small hump in the Re20_IMP TG curve at $T \approx 319$ °C to the contribution of the < 3 wt. % $La_6W_2O_{15}$ phase in Re20_IMP. In the TG curves of Mo10, Mo15 and Mo20(2) shown in Fig. 2c, clear fingerprints of the La_2O_3 phase

can be noticed. Among the phase-pure LWMoO specimens, the lowest Δm has been measured for Mo20(1), $\Delta m^{Mo20(1)}$ = 0.153(4) wt. %. In Fig. 2c, a slight decrease in mass loss with increasing Mo substitution can be ascertained. The finding that Δm^{Mo5} is slightly higher than Δm^{Mo1} is rationalized by the non-equivalent La/(W+Mo) ratio (see Fig. 1b). However, the mass loss decrease seen for LWMoO with increasing Mo substitution is much lower than that measured for LWReO with increasing Re substitution. While the mass loss of Mo20(1) ($\Delta m^{Mo20(1)}$ = 0.153(4) wt. %) is similar to the mass loss of LWO54P (Δm^{LWO54P} = 0.159(3) wt. %), the mass loss for the sample Re20_IMP (Δm^{Re20_IMP} = 0.080(6) wt. %) is about half the value. Mo20(1) and Re20_IMP have been compared due to their similar stoichiometry and substitution level on the W site (see Fig. 1). These results reveal that the oxidation state of Mo in oxidized conditions is similar to that of W (W^{6+}) and lower than Re (Re^{7+}), see discussion below. No useful information, however, can be extracted from the La_2O_3-containing specimens (Mo10, Mo15, Mo20(2)). Due to the Δm of the $La(OD)_3$ secondary phase ($\Delta m^{La(OD)3}$ = 9.680(8) wt. %) more than 50 times larger than the main LWO phase and also its different onset temperature T_i, $La(OD)_3$ even in small amounts alters both the onset temperatures T_i and the mass loss Δm of the LWO specimens appreciably (about a factor two for Mo10). In Table 2 the mass loss is shown together with the onset temperature T_i, determined from TG measurements under dry conditions. This relation is also plotted in Fig. 3.

Table 2. Mass loss Δm and onset temperature T_i determined from TG measurements.

Label	Δm (wt. %)	T_i (°C)
LWO54P	0.159(3)	337(3)
LWO52	0.079(4)	353(3)
LWO53	0.110(4)	345(3)
LWO54	0.153(5)	348(3)
LWO54.5	0.174(4)	338(3)
LWO55	0.182(5)	345(3)
LWO56	0.242(3)*	314(3)
Re02	0.196(4)	305(3)
Re05	0.194(3)	306(3)
Re1	0.155(4)	326(3)
Re5	0.135(3)	335(3)
Re10	0.121(5)	324(3)
Re15	0.112(5)	324(3)
Re20_IMP	0.080(6)	338(3)
Re20	0.208(6)*	283(3)
Mo1	0.173(4)	325(3)
Mo5	0.178(3)	316(3)
Mo10	0.281(6)*	--
Mo15	0.233(4)*	--
Mo20(1)	0.153(4)	308(3)
Mo20(2)	0.219(6)*	289(3)
La_2O_3	9.680(8)	305(3)
$La_6W_2O_{15}$	0.072(5)	252(3)

* Δm overestimated due to La_2O_3 secondary phase

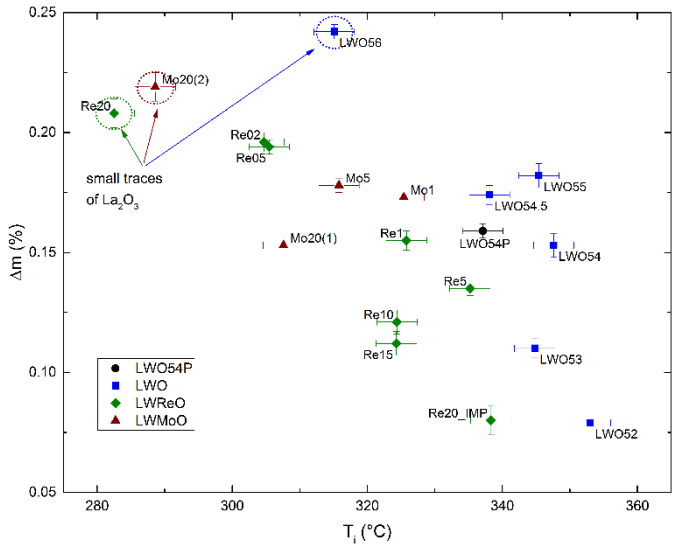

Fig. 3. Water uptake Δm as a function of the onset temperature T_i for the investigated sample series. The data points inside the dotted circles denote the specimens with some La_2O_3 secondary phase, which thus are not representative because of the non-negligible contribution to mass loss and onset temperature of $La(OD)_3$.

The interpretation and discussion of TG results in combination with the composition studies in LWO and LW*M*O specimens is clarified in Fig. 4, recalling first the charge compensation model for LWO according to the literature [20, 22, 28].

The general chemical formulation for LWO is expressed by:

$$La_{28-x}W_{4+x}O_{54+\delta}v_{2-\delta}\ , \tag{1}$$

where $\delta = 3x/2$ and v denotes the number of vacancies per unit cell. According to Magraso, *et al.* [22], δ defines the oxygen content which compensates the $W_{La2}^{\bullet\bullet\bullet\bullet}$ donors. $W_{La2}^{\bullet\bullet\bullet\bullet}$ is the substitution on a La2 site by a W2 donor, expressed in the Kröger-Vink (K-V) notation. Therefore, at a given x (or a given La/W ratio), it is possible to estimate by charge compensation the amount of vacancies in the unit cell. For increasing La/W ratio, charge compensation predicts an increase of vacancy concentration, confirming the results presented earlier (Fig. 2*a*). The reaction of LWO upon deuteration is expressed by reactions (2) and (3)

$$La_{28-x}W_{4+x}O_{54+\delta}v_{2-\delta} + yD_2O \overset{water\ splitting}{\longleftrightarrow} (OD)_y + D_y + La_{28-x}W_{4+x}O_{54+\delta}v_{2-\delta}\ , \tag{2}$$

$$(OD)_y + D_y + La_{28-x}W_{4+x}O_{54+\delta}v_{2-\delta} \overset{OD,\ D\ taken\ up}{\longleftrightarrow} La_{28-x}W_{4+x}O_{54+\delta+y}D_{2y}v_{2-\delta-y}\ , \tag{3}$$

where y, the amount of dissolved water, is calculated from the mass loss according to Schober and Friedrich [37]. y corresponds to the number of OD groups per unit cell taken up during deuteration

$$y = c_{D_2O} = \frac{\Delta m\ (\%)}{100} \times \frac{M_{LWO}}{M_{D_2O}} \leq 2 - 3x/2\ , \quad (4)$$

where the D_2O number of molecules (c_{D_2O}) per unit cell is equal to the number of OD groups per unit cell. In Fig. 4, the amount of vacancies obtained from TG and calculated using the charge compensation model reported for LWO [20, 22, 28] are presented as a function of the La/(W+*M*) ratio (values from Fig. 1 and Fig. 2). In Fig. 4, c_{D_2O} or, in other words, the vacant oxygen sites filled during deuteration ($v_{unit\ cell}^{oxygen}$) were calculated according to Eq. (4) and are reported as a function of the La/(W+*M*) ratio.

Firstly, in Fig. 4 it can be noticed that the experimentally determined water uptake of LWO can be approximately represented by a linear trend in the region of the investigated La/W ratios (R^2 = 0.95, not presented). The specimen with the highest La/W ratio (LWO56, inside the blue dotted circle) contains less than 1 wt. % La_2O_3. Some La_2O_3 impurities were also found in Re20 and Mo20(2), whose corresponding data points are depicted in Fig. 4 inside the green and brown dotted circles, respectively. This shifts the calculated water uptake for LWO56, Re20 and Mo20(2) towards higher values due to the high hygroscopicity of the secondary La_2O_3 phase. Two data points belonging to the non-substituted LWO system were taken from the literature [28] and are depicted in open black squares in Fig. 4. Of those two data points at La/W = 5.3 and La/W = 5.6, the latter matches with the experimental values found in the present work. However, the former deviates from all data of the present work, being the sole agreeing with the theoretical predictions of the chemical formulation (1). Even if small shifts in La/W ratio due to possible systematic errors in the EPMA measurement calibrations on the LWO54P specimen cannot be entirely excluded, it is reasonable to say that the data point from literature [28] matching the theoretical prediction may correspond to a different composition. This statement cannot be proven as sample composition studies were not included in Hancke, *et al.* [28], who claim that the data point at La/W = 5.6 (open black square, centre of Fig. 4) does not match the theoretical calculations (red dotted line) because either some segregation of La_2O_3 could occur and lower the hydration of LWO, or a certain extent of vacancy ordering exists. The former statement is proven to be wrong by the properties of La_2O_3. Concerning the latter statement, it is not expected that vacancy ordering could appear when one single unit cell is composed in average by about 86 atoms and 0.5 vacancies. However, that vacancy ordering does not subsist cannot be univocally excluded.

Likewise for the LWO system, a difference between the number of calculated and experimentally determined oxygen vacancies in the LW*M*O unit cell can be noticed. It is recalled that the humidification treatments were performed under wet(D_2O) argon gas whilst the TG measurements were performed in dry argon gas (reducing atmosphere). For LWReO specimens, the deviation of the vacancy concentration from theory (red dotted line in Fig. 4) is even larger than for the LWO system and shows a systematic trend to lower vacancy concentrations with increasing Re substitution at constant La/(W+Re) ratio. This has been rationalized as a larger oxidation state of Re compared to W, i.e. Re^{7+} compared to W^{6+} [26]. This result will be shortly recalled below. In contrast to the LWReO system, the vacancy concentration in LWMoO specimens seems to be only slightly dependent on Mo substitution and lies at

about the same value of vacancy concentration as that of the LWO system with the same La/(W+Mo) ratio. Eqs. (1-4) can be extended to Mo-containing specimens, leading to the following interpretation for the effect of Mo substitution in LWO: as the vacancy concentration in LWMoO specimens obtained from TG agrees with that for LWO and only slightly depends on Mo substitution, the excess charge of Mo should be equal to that of W ($Mo_{La2}^{\bullet\bullet\bullet}$ in K-V). Thus, in its oxidized state, the oxidation state of Mo is mainly +6 (Mo^{6+}). After TG, Mo might have been reduced to Mo^{5+} or Mo^{4+} as reported in temperature-programmed reduction (TPR) studies for dry H_2 (10 % in Ar) atmosphere [9] and in XPS measurements for as sintered and reduced $Nd_{5.5}W_{(1-y)}Mo_yO_{12-\delta}$ [14].

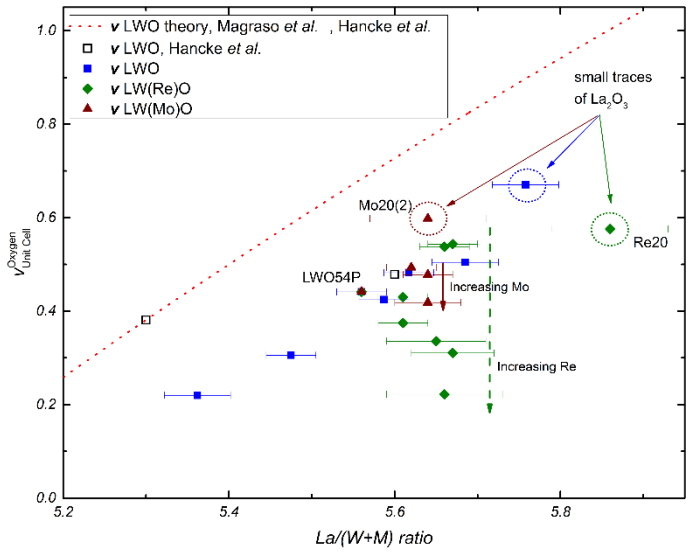

Fig. 4 Filled oxygen vacancies as obtained from TG (full symbols) as a function of the La/(W+*M*) ratio. The theoretical amount of oxygen vacancies in LWO (red dotted line) was calculated according to the charge compensation equation derived from chemical formulation (1) [22, 28], while Eq. 4) was employed to calculate the oxygen vacancy concentration from TG measurements. The two values for LWO from Hancke, *et al.* [28] are shown in open black squares. The data points inside the dotted circles denote the specimens with some La_2O_3 secondary phase, which thus are not representative because of the non-negligible contribution to mass loss of $La(OD)_3$.

In contrast to the LWMoO system, a clear trend of decreasing vacancy concentration with increasing Re substitution was found for the LWReO system. This is in line with the higher oxidation state of Re compared to W when Re is oxidized, i.e., as-sintered or oxidized LWReO could contain Re^{7+} and Re^{6+} cations. If the TG measurement is carried out under reducing conditions, the higher reducibility of Re compared to W [9] should change the Re oxidation state from $Re^{7+/6+}$ to $Re^{5+/4+}$. From the results of the diffraction measurements shown by Fantin, *et al.* [26] and Fantin [38] it can be concluded that the O_1 site bonded to the 4*a* site (W_1/Mo_1 or W_1/Re_1, see Fig. S2, *SI†*) does not exhibit vacancies in any of the LW*M*O (*M* = Mo, Re) systems. Therefore, substitution of W_1 by Mo_1 or Re_1 does not change the octahedral coordination, resulting for W_1, Mo_1 and Re_1 in a coordination number of *N* = 6. However, the oxidation state of the substituted Mo_1 or Re_1 on W_1 site remains unclear, as, in principle, octahedral coordination is possible for all the allowed oxidation states (+3 to +6 for Mo, +4 to +7 for Re)[39]. Nevertheless, as the vacancies contributing to hydration (deuteration) and the ensuing measured mass change sit only on the 32*f* Wyckoff site bonded to the La2/W2/*M*2 48*h* site, it is expected that Re^{7+} in LWReO and Mo^{6+} in LWMoO occupy at least the 48*h* site ($Re_{La2}^{\bullet\bullet\bullet\bullet}$ and $Mo_{La2}^{\bullet\bullet\bullet}$ in K-V). In LWReO, this results in $\delta_{Re} = 4/2x_{Re} = 2x_{Re}$ and $v_{Re} = 2 - 2x_{Re}$ (cf. Eqs. (1-4)), where x_{Re} is the Re amount on the 48*h* site. In LWMoO, this results in $\delta_{Mo} = 3/2x_{Mo}$ and $v_{Mo} = 2 - 3/2x_{Mo}$ (cf. Eqs. (1-4)), where x_{Mo} is the Mo amount on the 48*h* site. This means that Re^{7+} in the structure replacing W^{6+} in LWO on the 48*h* site

theoretically results in a lower vacancy concentration ($v_{Re} < v_W$), while Mo^{6+} replacing W^{6+} in LWO results in a similar vacancy concentration ($v_{Mo} \approx v_W$). This interpretation explains the results shown in Fig. 4.

The discussion above concerns TG results on oxidized/deuterated specimens with the mass loss obtained under reducing conditions. The oxidation states of Re and Mo in the oxidized specimen are supposed to be $Re^{7+/6+}$ and Mo^{6+}, respectively, before TG is carried out. It is expected that Re and Mo reduce to $Re^{5+/4+}$ and $Mo^{5+/4+}$, respectively, during TG and during the drying procedure in the furnace (cf. experimental part). However, whether Mo/Re reduction during TG influences the experimental and/or theoretical vacancy concentration and plays a role in the deviation between model and results is not yet clear even for W in the parent compound LWO. Nevertheless, it is possible to infer more information on oxidation and reduction of *M* = Mo, Re ions in LW*M*O specimens by evaluating and comparing the lattice parameters of dry(Ar) and D_2O(Ar) specimens as a function of the La/(W+*M*) ratio, as presented in Fig. 5a and Fig. 5b, respectively.

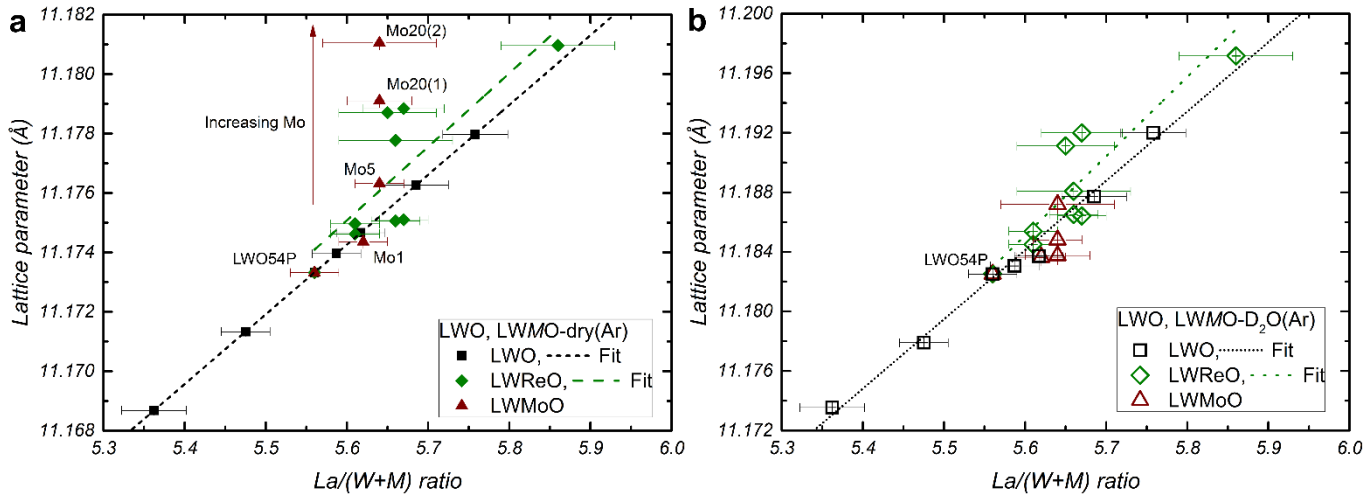

Fig. 5 Lattice parameters of LWO and LW*M*O in (*a)* dry(Ar) and (*b)* D_2O(Ar) conditions, as a function of the La/(W+*M*) ratio. The lattice parameters in dry(Ar) conditions of the LWO and LW*M*O specimens were extracted from the patterns represented in Fig. S1. Fits are straight lines.

For La/(W+Mo) ratios between 5.56 and 5.63, the lattice parameter of the dry(Ar) specimens increases with increasing La concentration. At La/(W+Mo) ≈ 5.65 the lattice parameter increases with increasing Mo concentration at constant La/(W+Mo) ratio. From this result it can be inferred that the average size of the substituting Mo in reducing conditions is higher than that of the substituted W. Thus, during the drying procedure, Mo can be reduced to Mo^{5+} ($R_i(Mo)_{5+}^{6fold}$ = 0.63 Å) and/or Mo^{4+} ($R_i(Mo)_{4+}^{6fold}$ = 0.65 Å), larger than W, ($R_i(W)_{6+}^{6fold}$ = 0.60 Å). It is assumed that Mo^{4+} does not reduce further according to TPR studies performed under more reducing conditions than in the present work [9]. The lattice parameters reported in Fig. 5 are a consequence of specimen drying at oxygen concentrations of about 10^{-12} (measured at *T* = 25 °C) compared to that of a TG measurement, estimated to lie in the 10^{-5}-10^{-4} range (*T* = 22 °C). Moreover, drying has been performed for longer times (4 h at 900 °C) compared to the TG measurement (< 2 h at 10 K/min heating rate up to 1000 °C). Therefore, reduction during the drying procedure is expected to be higher than during TG. Such an argument could also be applied for Re substitution in LWO. Re cations are more reducible than Mo and may exist in many different oxidation states upon reduction ($Re^{7+/6+}$ →

$Re^{5+/4+}$). At T = 900 °C, following the TPR studies reported [9], most of the Re cations should have the oxidation state Re^{4+}, ($R_i(Re)_{4+}^{6fold}$ = 0.63 Å), with a possible contribution of the Re^{5+} oxidation state ($R_i(Re)_{5+}^{6fold}$= 0.58 Å). As $R_i(Re)_{4+}^{6fold}$ = 0.63 Å > 0.60 Å = $R_i(W)_{6+}^{6fold}$, but also $R_i(Re)_{5+}^{6fold}$ = 0.58 Å < 0.60 Å = $R_i(W)_{6+}^{6fold}$, this could explain the slight increase in the dry(Ar) lattice parameters upon Re substitution and for the same La/(W+Re) ratio. Regarding the lattice parameters of the deuterated specimens (Fig. 5b) and comparing these lattice parameters with the TG results shown in Fig. 2 and Fig. 4, the oxidized Re and Mo are expected to have $Re^{7+/6+}$ and Mo^{6+} oxidation states, respectively, and, therefore, smaller ionic radii than W. This would result in smaller lattice parameters for LW*M*O-D_2O(Ar) compared to LWO-D_2O(Ar) specimens, which should increase as lattice(LWReO) < lattice(LWMoO) < lattice(LWO) or $R_i(Re)_{7+,6+}^{6fold} < R_i(Mo)_{6+}^{6fold} < R_i(W)_{6+}^{6fold}$. However, the oxygen atoms / OD groups filling the vacant oxygen sites also contribute to the unit cell size due to anion-anion repulsion and cation rearrangements, which results in an increasing unit cell size with increasing number of filled vacancies. As inferred from TG studies at constant La/(W+*M*) ratio, the amount of vacant sites filled by charge compensation (δ in Eqs. (1-4)) points in the opposite direction than the lattice parameters, being δ(LWO) ≈ δ(LWMoO) < δ(LWReO), or δ(W^{6+}) ≈ δ(Mo^{6+}) < δ($Re^{7+/6+}$) and compensate the decrease due to changes in ionic radii. The discussion above represents the present understanding of such systems as many free parameters have to be properly evaluated to provide a complete comprehension of the LWO and LW*M*O systems, such as the different La/(W+*M*) ratio, substitution degree, reducing/oxidizing atmospheres, time and temperature. It can be concluded, however, that an answer to the discrepancies observed between the defect chemistry calculations and the vacancy concentration established with the TG data in LWO and LW*M*O is, at present, still missing. Besides, it has been noticed that in many publications on LWO and LW*M*O that report composition studies with EPMA, as in the present work, the measured La/(W+*M*) ratios for most of the specimens are slightly shifted from the nominal to higher values [20, 24, 25, 27, 29]. If this shift of the composition is neglected the LWO/LW*M*O properties in terms of, e.g., oxygen vacancy prediction (see Fig. 4) or conductivity may lead to erroneous interpretations of the results. The reasons for the minor differences in La/(W+*M*) ratio are ascribed to evaporation of W during LWO / LW*M*O synthesis [15, 29] and/or due to segregation of W-rich phases at the specimen surface. Moreover, for some specimens (e.g. Re20, but to a minor extent also LWO54P and others) segregation of La_2O_3 occurs during annealing (see literature for LWO [20]). This is another variable to take into account as La_2O_3 segregation may substantially alter the specimen's water uptake and composition. Direct evidence of La_2O_3 segregation can be shown for the Re20 specimen by depicting the corresponding X-ray diffraction patterns taken at different time periods (see Fig. S5, *SI†).* More information on this feature may be ascertained by comparing the elemental maps of LWO54P, Re20 and Mo20(2) measured by EPMA and shown in the Supporting Information (Fig. S6, *SI†*). Here, the elemental maps were collected from pieces of the sintered pellets after polishing. Hence, these maps represent the specimen in the as-sintered condition. The relative intensity scale used by each detector is also presented and can be used for comparison within a single elemental image. As neither La-rich regions (fingerprint of La_2O_3), nor W(Mo/Re)-rich regions are visible in the maps of the elements constituting LWO54P, Re20 and Mo20(2), the specimen's homogeneity is confirmed in the as-sintered state on the micrometer scale. This

finding suggests that the secondary phases observed by XRD/TG measurements in Re20, but also to a minor extent in LWO54P and Mo20(2) have been induced by repeated annealing.

4. Summary and conclusions

This work shows the relation between the composition and the oxygen vacancy concentration in non-substituted $La_{6-x}WO_{12-\delta}$ ($0.4 \leq x \leq 0.8$) (LWO) and substituted $La_{5.4}W_{1-y}M_yO_{12-\delta}$ ($0 \leq y \leq 0.2$; M = Mo, Re) samples. Most of the specimens investigated belong to the single-phase region. In LWO, an increasing La/W ratio leads to a systematic increase of vacant oxygen sites and a decrease of onset temperature T_i, though even less than 1 wt. % La_2O_3 impurities may substantially alter both the water uptake and T_i. T_i decreases with increasing vacancy concentration and thus a higher vacancy concentration in the specimen is related to a reduced stability of the crystal structure. Clear evidence for the presence of the secondary phases $La_6W_2O_{15}$ and La_2O_3 was found in the thermogravimetric curves. Thermogravimetry appears more sensitive than conventional X-ray diffraction in resolving contributions especially from the highly hygroscopic La_2O_3. La_2O_3 segregation has been observed after repeated annealing in reducing conditions (dry(Ar)) in specimens with high La/(W+M) ratios, independently of M, such as in $La_{5.86}W_{0.83}Re_{0.17}O_{12-\delta}$. A clear discrepancy between the current theoretical model for the LWO defect structure and the experimental data was found being also present in M-substituted LWO systems. The comparison between diffraction and thermogravimetric results on LWMO and LWO systems leads to the interpretation that in LWMO, the oxidation states of Re and Mo ions are $Re^{7+/6+}$ and Mo^{6+} in oxidizing conditions, and $Re^{5+/4+}$ and $Mo^{5+/4+}$ in reducing conditions. However, the discrepancy between theory and experiment in the $La_{6-x}WO_{12-\delta}$ ($0.4 \leq x \leq 0.8$) parent compound cannot be clearly explained and therefore requires further investigations.

Acknowledgements

We thank C. Leistner and C. Förster (HZB) for their help in performing TG and XRD experiments and in sample preparation. The Helmholtz Association funded this work through the Helmholtz Alliance MEM-BRAIN (Initiative and Networking Fund).

Literature

[1] B. Sorensen, *Int. J. Hydrogen Energy* **32** (2007) (10-11) 1597.
[2] T. Ho, V. Karri, *Int. J. Hydrogen Energy* **36** (2011) (16) 10065.
[3] A. Genovese, N. Contrisciani, F. Ortenzi, V. Cazzola, *Int. J. Hydrogen Energy* **36** (2011) (2) 1775.
[4] M. Kim, Y.-J. Sohn, C.-W. Cho, W.-Y. Lee, C.-S. Kim, *Journal of Power Sources* **176** (2008) (2) 529.
[5] T. Niknam, M. Bornapour, A. Gheisari, *Energy Conversion and Management* **66** (2013) 11.
[6] D. Wang, S. Chen, C. Xu, W. Xiang, *Int. J. Hydrogen Energy* **38** (2013) (13) 5389.
[7] M. Pérez-Fortes, J.C. Schöneberger, A. Boulamanti, E. Tzimas, *Applied Energy* **161** (2016) 718.
[8] M. Peters, B. Kohler, W. Kuckshinrichs, W. Leitner, P. Markewitz, T.E. Muller, *ChemSusChem* **4** (2011) (9) 1216.
[9] S. Escolastico, J. Seeger, S. Roitsch, M. Ivanova, W.A. Meulenberg, J.M. Serra, *ChemSusChem* **6** (2013) (8) 1523.
[10] Y. Chen, S.F. Cheng, L. Chen, Y.Y. Wei, P.J. Ashman, H.H. Wang, *Journal of Membrane Science* **510** (2016) 155.
[11] S. Escolastico, C. Solis, T. Scherb, G. Schumacher, J.M. Serra, *Journal of Membrane Science* **444** (2013) 276.
[12] S. Escolastico, C. Solis, J.M. Serra, *Solid State Ionics* **216** (2012) 31.
[13] S. Escolastico, C. Solis, C. Kjolseth, J.M. Serra, *Energy & Environmental Science* **7** (2014) (11) 3736.
[14] S. Escolastico, S. Somacescu, J.M. Serra, *Journal of Materials Chemistry A* **3** (2015) (2) 719.
[15] S. Escolastico, S. Somacescu, J.M. Serra, *Chem. Mater.* **26** (2014) (2) 982.

[16] J. Seeger, M.E. Ivanova, W.A. Meulenberg, D. Sebold, D. Stover, T. Scherb, G. Schumacher, S. Escolastico, C. Solis, J.M. Serra, *Inorg Chem* **52** (2013) (18) 10375.
[17] J. Seeger, Entwicklung protonenleitender Werkstoffe und Membranen auf Basis von Lanthan-Wolframat für die Wasserstoffabtrennung aus Gasgemischen, Ruhr-Universität Bochum, Bochum (2013).
[18] R. Haugsrud, *Solid State Ionics* **178** (2007) (7-10) 555.
[19] A. Magraso, C. Frontera, *Dalton Trans* (2016).
[20] A. Magraso, R. Haugsrud, *Journal of Materials Chemistry A* **2** (2014) (32) 12630.
[21] A. Magraso, C.H. Hervoches, I. Ahmed, S. Hull, J. Nordstrom, A.W.B. Skilbred, R. Haugsrud, *Journal of Materials Chemistry A* (2013).
[22] A. Magraso, J.M. Polfus, C. Frontera, J. Canales-Vazquez, L.E. Kalland, C.H. Hervoches, S. Erdal, R. Hancke, M.S. Islam, T. Norby, R. Haugsrud, *J. Mater. Chem.* **22** (2012) (5) 1762.
[23] S. Erdal, L.E. Kalland, R. Hancke, J. Polfus, R. Haugsrud, T. Norby, A. Magraso, *Int. J. Hydrogen Energy* **37** (2012) (9) 8051.
[24] A. Magraso, C. Frontera, D. Marrero-Lopez, P. Nunez, *Dalton Trans* (2009) (46) 10273.
[25] T. Scherb, Strukturelle Charakterisierung von Wasserstoff trennenden Gasseparationsmembranen auf Lanthanoid-Wolframat-Basis, Technische Universität Berlin, Berlin (2011), p.139.
[26] A. Fantin, T. Scherb, G. Schumacher, J. Seeger, M.E. Ivanova, U. Gerhards, W.A. Meulenberg, R. Dittmeyer, J. Banhart, *Journal of Applied Crystallography* **49** (2016) (5) 1544.
[27] T. Scherb, S.A.J. Kimber, C. Stephan, P.F. Henry, G. Schumacher, S. Escolástico, J.M. Serra, J. Seeger, J. Just, A.H. Hill, J. Banhart, *Journal of Applied Crystallography* **49** (2016) (3) 997.
[28] R. Hancke, A. Magrasó, T. Norby, R. Haugsrud, *Solid State Ionics* **231** (2013) (0) 25.
[29] M. Amsif, A. Magraso, D. Marrero-Lopez, J.C. Ruiz-Morales, J. Canales-Vazquez, P. Nunez, *Chem. Mater.* **24** (2012) (20) 3868.
[30] M.P. Pechini, Method of preparing lead and alkaline earth titanates and niobates and coating method using the same to form a capacitor, SPRAGUE ELECTRIC CO, United States (1967).
[31] M. Yoshimura, A. Rouanet, *Materials Research Bulletin* **11** (1976) (2) 151.
[32] L.L.Y. Chang, M.G. Scroger, B. Phillips, *J Inorg Nucl Chem* **28** (1966) (5) 1179.
[33] L.L.Y. Chang, B. Phillips, *Inorg. Chem.* **3** (1964) (12) 1792.
[34] J.S.O. Evans, *Materials Science Forum* **651** (2010) 1.
[35] B.H. Toby, *Journal of Applied Crystallography* **34** (2001) 210.
[36] L. Vegard, *Z Phys* **5** (1921) (1) 17.
[37] T. Schober, J. Friedrich, *Solid State Ionics* **113–115** (1998) 369.
[38] A. Fantin, Structural characterisation of nonsubstituted and Mo- or Re-substituted proton-conducting $La_{6-x}WO_{12-d}$ by diffraction of X-rays and neutrons, Technische Universität Berlin, Berlin (2016), p.125.
[39] R.D. Shannon, *Acta Crystallogr A* **32** (1976) (Sep1) 751.